Ni(OH)$_2$ Decorated Pt-Cu Octahedra for Ethanol Electrooxidation Reaction

Youngmin Hong[†], Hee Jin Kim[†], Hye Jin Lee, Jeonghyeon Kim and Sang-Il Choi*

Department of Chemistry and Green-Nano Materials Research Center, Kyungpook National University, Daegu, South Korea

Here we report the synthesis of 9 nm Ni(OH)$_2$ decorated Pt-Cu octahedra (Ni(OH)$_2$-PtCu) in one-pot synthesis for ethanol oxidation reaction (EOR) electrocatalysis in acidic electrolyte. To prepare Ni(OH)$_2$-PtCu octahedra, CO gas was directly introduced in a reaction process as selective capping agents on the PtCu(111) facet. Ni(OH)$_2$ was naturally deposited on the Pt-Cu octahedra during the synthesis. Carbon supported Ni(OH)$_2$-PtCu (Ni(OH)$_2$-PtCu/C) as an EOR catalyst showed enhanced CO tolerance due to the existence of oxophilic Ni(OH)$_2$ on the surface of Pt-Cu, facilitating water dissolution to produce OH adsorption and to promote complete CO oxidation to CO$_2$. In addition, Pt-Cu alloy composition also showed improvement of CO tolerance because of modified d-band structure of the Pt atoms, thereby weakening the binding strength of CO on the catalysts. Therefore, the Ni(OH)$_2$-PtCu/C showed enhanced EOR activity and durability compared to the Pt-Cu octahedra and commercial Pt/C counterparts.

Keywords: copper, platinum, nickel hydroxide, octahedra, ethanol oxidation

INTRODUCTION

Direct alcohol fuel cell (DAFC) for numerous applications has attracted huge attention due to its high efficiency under ambient operating conditions (Xu and Zhang, 2014; Ozoemena, 2016). For the anodic reaction of DAFC, ethanol has been received great interests for its utilization owing to its high energy density (8 kWh kg^{-1}), low toxicity, and ease of supply from agricultural products and biomass (Li and Pickup, 2006; Xu and Zhang, 2014). In addition, ethanol can be easily stored and transported for the practical uses compared to H$_2$ gas (Zhou et al., 2003; Kowal et al., 2009). During the ethanol oxidation reaction (EOR) in fuel cells, ethanol is consumed to generate electrical energy, and CO$_2$ is generated as a product from complete oxidation of ethanol. In this process, 12 electrons are produced (CH$_3$CH$_2$OH + 3H$_2$O → 2CO$_2$ + 12H$^+$ + 12e$^-$) under the thermodynamic standard potential of 0.085 V (Colmati et al., 2009; Busó-Rogero et al., 2014). However, owing to the slow kinetics of the EOR, making large overpotential and concomitant intermediate such as CO that has toxicity to the environment and fuel cell electrode materials, a number of researches have been made on new catalysts for enhancing EOR kinetics, CO-tolerant, and CO oxidation to CO$_2$ (Neto et al., 2007; Busó-Rogero et al., 2014; Ozoemena, 2016).

Platinum (Pt) has been commonly used as an EOR catalyst due to its excellent properties in the adsorption and dissociation of ethanol (Wang et al., 2015). However, high-cost, low abundance in the Earth crust, and undesirable CO poisoning during the EOR have delayed the practical applications (Zhang et al., 2015; Ghavidel et al., 2017). Therefore, alloying Pt with transition metals, such as Ru, Sn, Pd, Ni, and Cu have been intensively studied to reduce the Pt use and to alleviate CO poisoning on the surface of Pt thus to enhance the electrocatalytic activity of EOR (Vigier et al., 2004; Colmenares et al., 2006; Wang et al., 2006; Ammam and Easton, 2013; Dutta and Ouyang, 2015; Zhu et al., 2015). In this Pt-based alloy nature, a bifunctional mechanism was

generally accepted to rationalize enhanced performance of EOR. Specifically, the transition metals (M) positioned near the surface Pt would dissociate the water molecule and act as an adsorbent for the produced OH on its surface site ($H_2O \rightarrow M\text{-}OH_{ads} + H^+ + e^-$) at lower potentials compared to Pt (Hsieh and Lin, 2009; Kowal et al., 2009). Then, the $M\text{-}OH_{ads}$ on the surface of catalyst can help the oxidation of CO to CO_2 on the neighboring Pt sites ($Pt\text{-}CO_{ads} + M\text{-}OH_{ads} \rightarrow CO_2 + H^+ + e^-$) (Koper, 2011; Erini et al., 2015). Moreover, the M alloyed into the lattice of Pt can modify electronic structure of Pt, resulting in the reduction of bonding strength of Pt and CO and thus increase of EOR performance (Zhang et al., 2016; Liu et al., 2018). Additionally, ternary nanostructured catalysts were also studied to derive ternary ensemble of each metals. For example, Pt-Rh-Sn and Pt-Rh-Ni ternary alloys possessing highly oxophilic Rh, Sn, and Ni elements have been introduced to further modify the property of Pt-based bimetallic catalysts (Erini et al., 2015). These results indicated that the surface modification of alloy catalyst with oxidation form of transition metals such as $Ni(OH)_x$ activates water dissociation and provides OH_{ads} at lower potentials than Pt (Cui et al., 2013a; Erini et al., 2015).

Recently, facet-dependent electrocatalytic EOR has been intensively studied with the nanocatalysts of unique morphologies (Lai and Koper, 2008; Koper, 2011; Solla-Gullon et al., 2011; Zhao et al., 2016). In the case of Pt-Ni alloy, octahedral Pt-Ni nanocatalysts enclosed by (111) facets showed 4.6 times higher EOR activity compared to spherical Pt-Ni consisted of mixed facets (Sulaiman et al., 2017). To the best of our knowledge, however, there has not much reports on ternary $Ni(OH)_2$-Pt-Cu electrocatalyst for EOR. In this context, we here successfully synthesized 9 nm $Ni(OH)_2$ decorated Pt-Cu octahedra in one-pot synthesis. We designed Pt-Cu octahedra as PtCu(111) alloy substrates and $Ni(OH)_2$ decorated on the surface of Pt-Cu octahedra as the site for OH_{ads}, improving water dissociation. The as-obtained $Ni(OH)_2$ decorated Pt-Cu octahedra showed enhanced catalytic EOR activity and durability compared to binary Pt-Cu octahedra and commercial Pt/C.

EXPERIMENTAL SECTION

Chemicals

Platinum(II) acetylacetonate [Pt(acac)$_2$, Pt 48.0%] and copper(II) acetylacetonate [Cu(acac)$_2$, 98%] were obtained from Alfa Aesar. Nickel(II) acetylacetonate [Ni(acac)$_2$, 95%], oleic acid (OAc, 90%), oleylamine (OAm, ≥98%), and benzyl ether (BE, 98%) were obtained from Sigma-Aldrich. All chemicals were used as received without further treatment.

Synthesis of Ni(OH)$_2$ Decorated Pt-Cu Octahedra (Ni(OH)$_2$-PtCu)

In a standard synthesis, a mixture of Pt(acac)$_2$ (20.0 mg), Cu(acac)$_2$ (13.3 mg), Ni(acac)$_2$ (10.0 mg), OAm (4.0 mL), OA (4.0 mL), and BE (2.0 mL) was heated to 190°C within 20 min under Ar atmosphere and magnetic stirring. When the temperature reached 190°C, CO gas was bubbled into the mixture with a flow rate of 1 mL min^{-1}, and Ar purging was stopped at the same time (Kang et al., 2010). The mixture was

then heated to 210°C at a heating rate of 4°C min^{-1} under CO bubbling and held at 210°C for 40 min without CO bubbling. The resulting suspension was cooled down to room temperature naturally, and the $Ni(OH)_2$-PtCu octahedra were precipitated out by sequential addition of toluene (5 mL) and ethanol (10 mL). The supernatant was discarded by centrifugation at 3,000 rpm for 5 min. The resulting $Ni(OH)_2$-PtCu octahedra were dispersed in toluene for further treatment.

Preparation of Ni(OH)$_2$-PtCu Octahedra Supported on Carbon (Ni(OH)$_2$-PtCu/C)

A suspension of $Ni(OH)_2$-PtCu octahedra was added into a toluene solution containing 31.5 mg of Vulcan XC-72 R carbon and kept under ultrasonic wave agitation for 2 h. The resulting $Ni(OH)_2$-PtCu/C catalyst was centrifuged 3 times with toluene at 3,000 rpm for 5 min, and then dried under Ar protection at room temperature.

Acetic Acid (HOAc) Treatment of Ni(OH)$_2$-PtCu/C Catalyst (PtCu/C-HOAc)

$Ni(OH)_2$-PtCu/C catalyst (10 mg) was dispersed in HOAc (10 mL; ≥99.7%, Sigma-Aldrich) and then heated at 60°C for 2 h under magnetic stirring. After heating, the catalyst was washed three times with ethanol and dried under Ar protection at room temperature.

Morphological, Structural, and Elemental Characterizations

Transmission electron microscopy (TEM) images were obtained using a HT 7100 microscope (Hitachi, Japan) operated at an acceleration voltage of 120 kV. High-resolution TEM and energy dispersive X-ray spectroscopy (EDS) studies were carried out in JEM-2100F (JEOL, Japan) and Titan G2 ChemiSTEM Cs Probe (FEI, USA) operated at an acceleration voltage of 200 kV. The metal contents in catalysts were determined using inductively coupled plasma-optical emission spectroscopy (ICP-OES, PerkinElmer, Optima 7300DV, USA). X-ray diffraction (XRD) patterns were obtained with a D2 phaser X-ray diffractometer (Bruker, USA). X-ray photoelectron spectroscopy (XPS) was carried out using a spectrometer (Thermofisher Scientific, USA) with Al Kα X-ray (1486.6 eV) as the light source. All spectra were aligned using the C-1s peak at 284.5 eV as reference.

Electrochemical Measurements

All electrochemical measurements were carried out using a standard three-electrode cell connected to potentiostats (CHI 600E from CH Instruments and VSP from Bio-Logic). A Ag/AgCl electrode was used as the reference electrode, and potential values were calibrated with respect to reversible hydrogen electrode (RHE). Pt mesh (1 × 1 cm^2) was used as a counter electrode. A glassy carbon disk (GC, 5 mm in diameter, PINE instrumentation) was used as a working electrode. The GC surface was previously polished using 0.05 μm Al$_2$O$_3$ suspension. Catalyst ink was prepared by mixing a specific amount of catalyst powder, deionized water (1.0 mL), isopropyl alcohol (0.25 mL), and 5 wt% nafion (5 μL) using ultrasonication for 10 min. The

ink (10 μL) was dropped on a GC electrode and dried to form a thin film. The final Pt loading of electrocatalyst on a GC electrode was 10.2 μg cm^{-2}. The each electrocatalyst loaded on electrode was pre-cycled in an Ar-saturated 0.1 M HClO$_4$ solution between 0.08 and 1.20 V at a scan rate of 100 mV s^{-1}, and then cyclic voltammograms (CVs) were recorded between 0.08 and 1.20 V at

a scan rate of 50 mV s^{-1} in an Ar-saturated 0.1 M HClO$_4$ solution at room temperature. In a typical CO stripping experiment, the electrode potential was held at 0.05 V for 5 min in a CO-saturated 0.1 M HClO$_4$ solution for a fully adsorption of CO on the catalyst surface followed by flowing Ar for another 10 min to remove the CO in the solution, and then the CO stripping curve was recorded
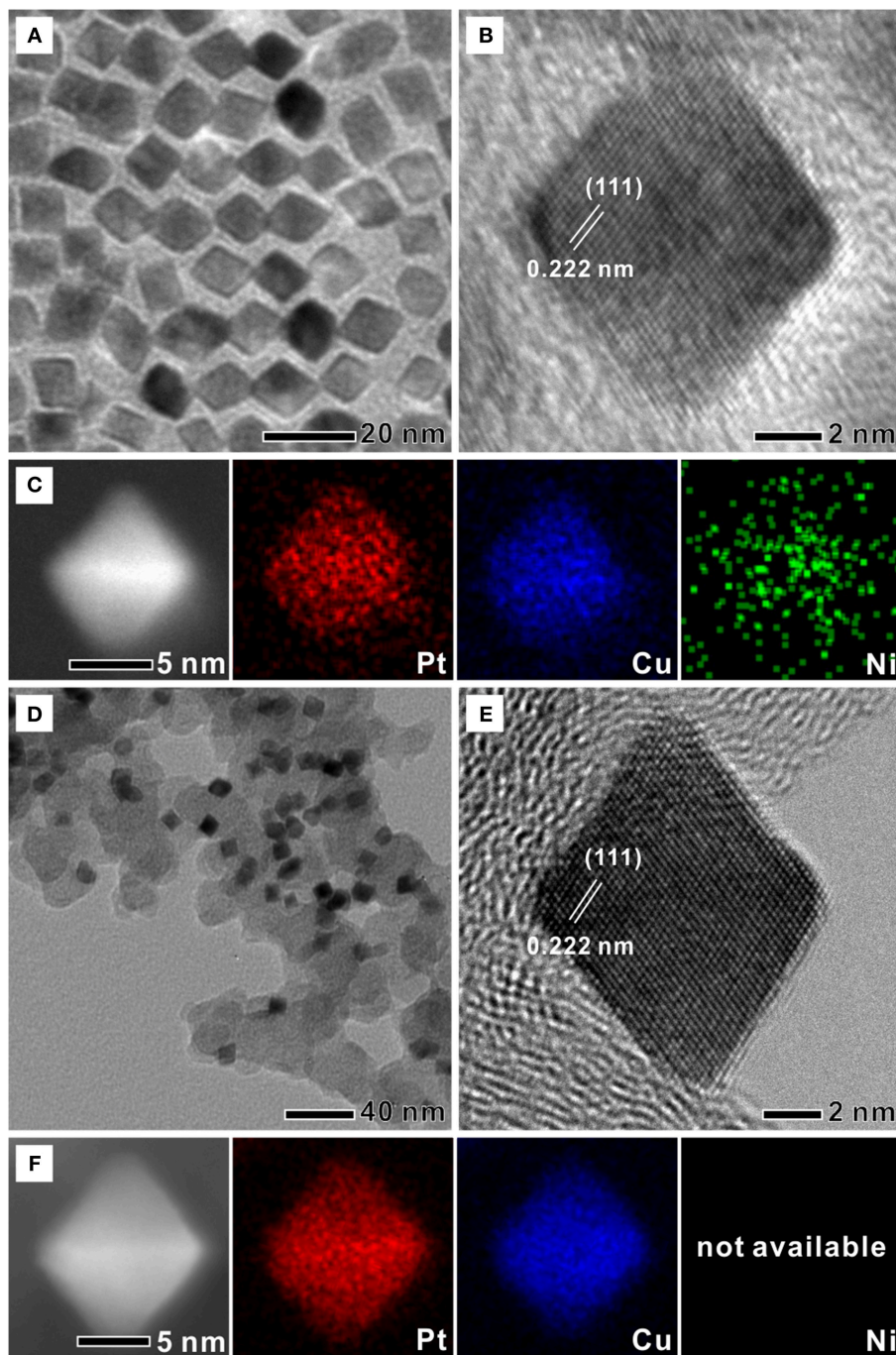

FIGURE 1 | TEM and high-resolution TEM images of (A,B) Ni(OH)$_2$ decorated Pt-Cu octahedra (Ni(OH)$_2$-PtCu) and (D,E) Ni(OH)$_2$ decorated Pt-Cu octahedra/C treated with acetic acid (PtCu/C-HOAc). STEM with corresponding EDS mapping images of (C) Ni(OH)$_2$-PtCu and (F) PtCu/C-HOAc.

by cycling between 0.08 and 1.20 V at 50 mV s^{-1}. For the EOR measurements, CV was conducted in an Ar-saturated solution containing 0.1 M HClO$_4$ and 1 M ethanol between 0.08 and 1.29 V at a scan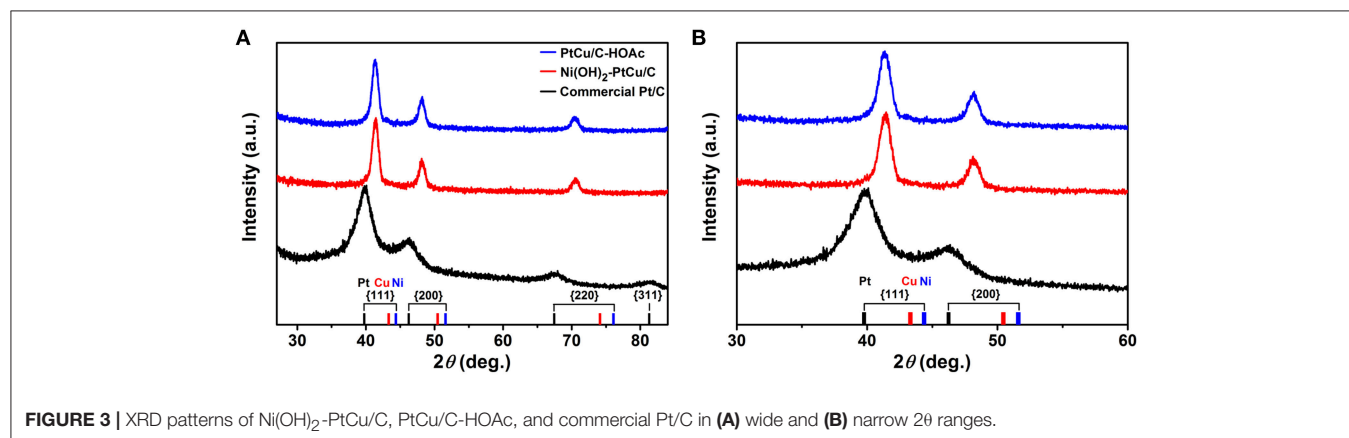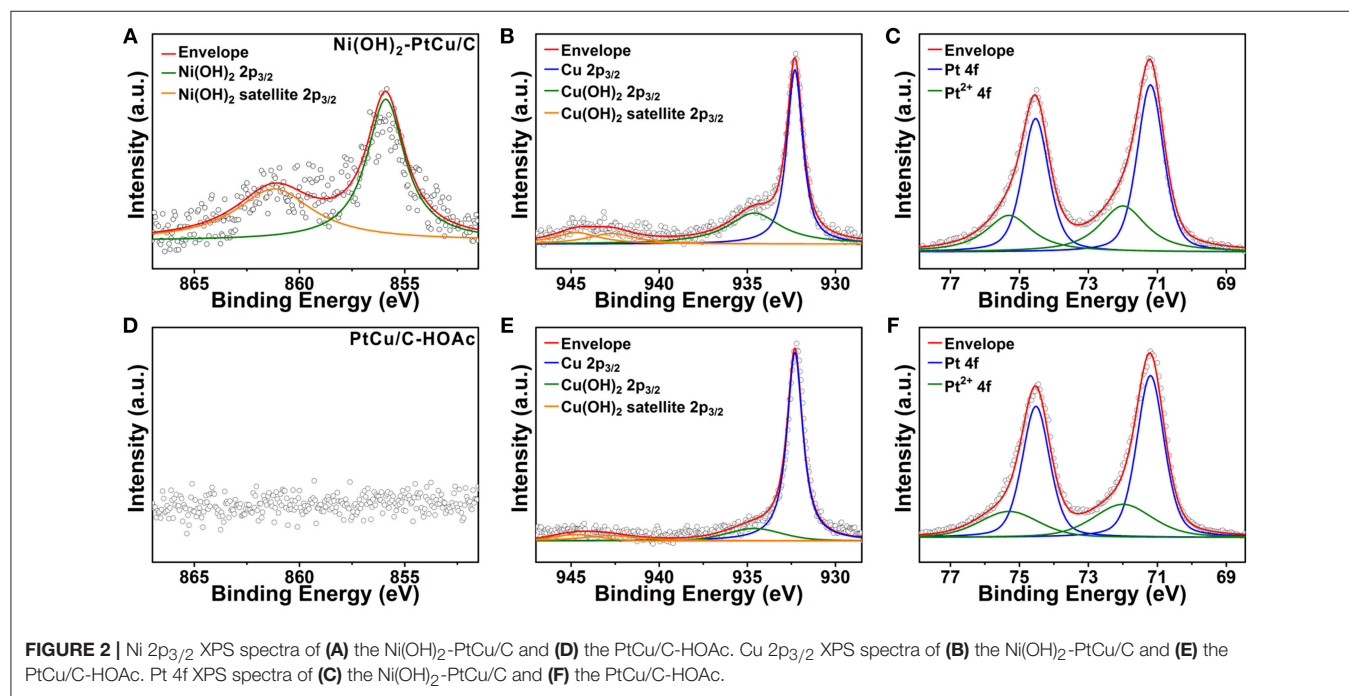 rate of 50 mV s^{-1}. Chrono-amperometry curve of the catalysts was recorded for 3000 s in an Ar-saturated 0.1 M HClO$_4$ and 1 M ethanol solution at 0.67 V. Long-term durability of the catalysts for EOR was performed in an Ar-saturated 0.1 M HClO$_4$ and 1 M ethanol solution by applying cyclic potential

TABLE 1 | Comparison of atomic ratio and Pt wt% in a catalyst obtained by ICP-AES, H$_{upd}$-based, and CO$_{ads}$-based electrochemical surface areas (ECSA$_H$, ECSA$_{CO}$), and onset potential of CO stripping.

Catalyst	Atomic ratio Ni: Pt: Cu	Pt wt% in a catalyst	ECSA$_H$ (m^2 g$_{Pt}^{-1}$)	ECSA$_{CO}$ (m^2 g$_{Pt}^{-1}$)	Onset potential of CO (V)
Commercial Pt/C	NA*	20**	60.29	66.83	0.80
Ni(OH)$_2$-PtCu/C	1.0: 2.1: 2.8	14.1	27.27	27.34	0.63
PtCu/C-HOAc	NA: 1.0: 1.0	14.9	28.06	30.85	0.67

*Not applicable.
**Nominal amount written in a tag.

FIGURE 2 | Ni 2p$_{3/2}$ XPS spectra of **(A)** the Ni(OH)$_2$-PtCu/C and **(D)** the PtCu/C-HOAc. Cu 2p$_{3/2}$ XPS spectra of **(B)** the Ni(OH)$_2$-PtCu/C and **(E)** the PtCu/C-HOAc. Pt 4f XPS spectra of **(C)** the Ni(OH)$_2$-PtCu/C and **(F)** the PtCu/C-HOAc.

FIGURE 3 | XRD patterns of Ni(OH)$_2$-PtCu/C, PtCu/C-HOAc, and commercial Pt/C in **(A)** wide and **(B)** narrow 2θ ranges.

sweep between 0.65 and 1.05 V at a scan rate of 100 mV s^{-1} for 2,000 cycles. Then, CV for EOR was recorded again in a fresh Ar-saturated 0.1 M HClO$_4$ and 1 M ethanol solution for comparison with the initial CV curve of EOR.

RESULTS AND DISCUSSION

In a typical synthesis of Ni(OH)$_2$-PtCu octahedra, a reaction mixture of Ni(acac)$_2$, Pt(acac)$_2$, Cu(acac)$_2$, OAc, OAm, and BE was heated to 190°C under Ar protection with magnetic stirring and then CO gas was bubbled into heated mixture with a flow rate of 1 mL min^{-1} while Ar purging was stopped. The mixture was heated again to 210°C, and CO bubbling was stopped when the temperature reached to 210°C. After the reaction was kept at 210°C for 40 min, a dark suspension including Ni(OH)$_2$-PtCu was obtained. In previous studies, CO gas released from metal carbonyls was used as a selective capping agent for {111} facets of Pt-Ni and Pt-Cu alloy nanocrystals under an OAm/OA co-surfactant system (Choi et al., 2013). However, use of transition metal carbonyl compounds can cause undesirable trace metal contaminations on the Pt catalysts through alloying and/or surface residues (Kang et al., 2010, 2013). Furthermore, transition metals released from metal carbonyls complicate the synthesis system, making it difficult to identify the formation mechanism of shape-controlled nanocrystals (Chang et al., 2017). Therefore, we here simply used CO gas as selective capping agent directly into the reaction mixture. **Figure 1A** shows TEM image of Ni(OH)$_2$-PtCu octahedra with an average edge length of 9.4 ± 1.1 nm. A TEM image on a large population of Ni(OH)$_2$-PtCu octahedra shows uniform size and shape (**Figure S1A**). High-resolution TEM (HRTEM) image of a single Ni(OH)$_2$-PtCu octahedron shows that the d-spacing for adjacent Pt lattice fringes measured from a few different sites was 0.222 nm, which is smaller than that of Pt{111} planes (0.227 nm) of face-centered cubic (fcc) bulk (**Figure 1B**) (Choi et al., 2013). Scanning transmission electron microscopy (STEM) with energy dispersive X-ray spectroscopy (EDS) mapping image confirmed well distributed Ni, Pt, and Cu elements in the single Ni(OH)$_2$-PtCu octahedron (**Figure 1C**). The Ni(OH)$_2$-PtCu octahedra loaded on carbon supports (Ni(OH)$_2$-PtCu/C) were shown in **Figure S1B**, indicating well-dispersed nanocrystals on carbon without aggregation. The Ni(OH)$_2$-PtCu/C was then treated with

HOAc at 60°C for 2 h. **Figures 1D,E** show TEM and HRTEM images of Ni(OH)$_2$-PtCu/C after HOAc treatment (PtCu/C-HOAc), respectively. After the acid treatment, the average edge length of PtCu/C-HOAc was 9.2 ± 1.1 nm and d-spacing for Pt lattice fringes was 0.222 nm, similar to the pristine Ni(OH)$_2$-PtCu octahedra. STEM with EDS mapping image of a single PtCu/C-HOAc shows an octahedral nanocrystal consisting of Pt and Cu but absence of Ni (**Figure 1F**).

To confirm the elemental composition of the as-prepared catalysts, ICP-AES was carried out and the resulting data are listed in **Table 1**. The ICP-AES results of Ni(OH)$_2$-PtCu/C and PtCu/C-HOAc indicate that Ni was fully removed and Cu was partially leached out during the HOAc treatment. Previous literatures on the Pt-based alloys have found that the transition metals in the Pt lattices cannot be completely removed during the acid treatment, but some are retained in the crystal structure (Chang et al., 2017; Park et al., 2017; Kwon et al., 2018; Kim et al., 2019). Therefore, in our case, we suggest that Ni was selectively deposited on the surface of Pt-Cu octahedra during the synthesis and was dissolved out when the Ni(OH)$_2$-PtCu/C catalyst was treated with HOAc. The Cu atoms on the surface of Ni(OH)$_2$-PtCu/C were also leached out and thus the surface composition of PtCu/C-HOAc is assumed to be Pt-rich.

To investigate chemical state of elements in catalysts, XPS was conducted. The Ni 2p$_{3/2}$ spectrum of Ni(OH)$_2$-PtCu/C shows a peak assigned to Ni(OH)$_2$ (855.9 eV) and Ni(OH)$_2$ satellite (861.2 eV), indicating the formation of Ni(OH)$_2$ on the surface of Ni(OH)$_2$-PtCu/C (**Figure 2A**) (Moulder, 1992). Meanwhile, Ni signal was not detected for PtCu/C-HOAc, revealing again that surface Ni(OH)$_2$ was dissolved when catalyst was treated with HOAc (**Figure 2D**). The Cu 2p$_{3/2}$ spectra of both Ni(OH)$_2$-PtCu/C and PtCu/C-HOAc showed a peak assigned to Cu(0) metal (932.3 eV), Cu(OH)$_2$ (934.6 eV), and Cu(OH)$_2$ satellite (942.7 and 944.7 eV) (**Figures 2B,E**) (Moulder, 1992). The Cu(OH)$_2$ peak was decreased after the HOAc treatment, indicating the surface Cu(OH)$_2$ leaching similar to Ni(OH)$_2$. The Pt 4f spectra of both catalysts show a peak fitted with doublets corresponding to Pt(0) metal (71.2 and 74.5 eV) and Pt^{2+} (72.0 and 75.3 eV) (**Figures 2C,F**) (Xia et al., 2012). **Figure 3A** shows XRD patterns in a wide 2θ range for commercial Pt/C, Ni(OH)$_2$-PtCu/C before and after HOAc treatment, representing fcc structure without other metal oxide
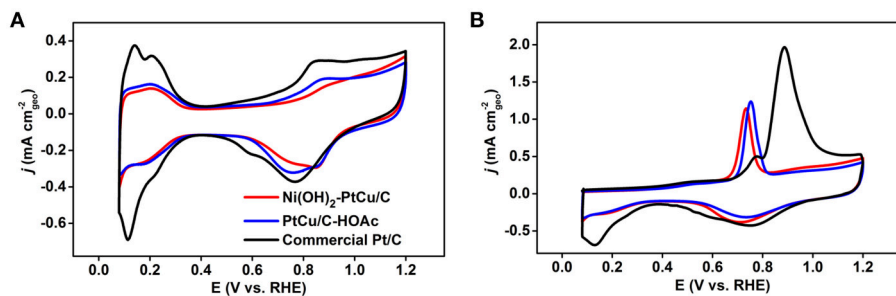

FIGURE 4 | (A) Cyclic voltammograms (CVs) and **(B)** CO stripping curves of the Ni(OH)$_2$-PtCu/C, the PtCu/C-HOAc, and the commercial Pt/C recorded in 0.1 M HClO$_4$ solutions with a scan rate of 50 mV s^{-1} at room temperature.

peaks. The narrow 2θ range window of the XRD shows diffraction peaks between Pt and Cu (**Figure 3B**), indicating that the decreased lattice spacing of Pt for Ni(OH)$_2$-PtCu/C and PtCu/C-HOAc compared to commercial Pt/C is the result of the presence of smaller Cu atoms in place of Pt atoms (Nosheen et al., 2013). Based on the observations, we understand the formation of Ni(OH)$_2$-PtCu octahedra during the standard synthesis. In the synthesis, Pt^{2+}, Cu^{2+}, and Ni^{2+} ions were initially decomposed out from the introduced metal precursors. Because of the difference of standard reduction potentials, Pt^{2+} (1.188 V) and Cu^{2+} ions (0.340 V) were primarily reduced to Pt and Cu metals forming Pt-Cu alloy nanocrystals but Ni^{2+} (−0.257 V)

FIGURE 5 | CVs of the Ni(OH)$_2$-PtCu/C, the PtCu/C-HOAc, and the commercial Pt/C normalized by **(A)** ECSA and **(B)** Pt loading recorded in Ar-saturated solutions containing 0.1 M HClO$_4$ and 1.0 M ethanol with a scan rate of 50 mV s^{-1} at room temperature. **(C)** Comparisons of the specific and mass activities toward the ethanol oxidation reaction of the three different catalysts measured at the potentials showing the maximum current density in forward scans.

was dissolved in the mixture. Under the CO gas, Pt-Cu octahedra enclosed by {111} facets were mainly produced, and then rest of Ni^{2+} was deposited on the surface of Pt-Cu as Ni(OH)$_2$ form (Zhang et al., 2015; Kavian et al., 2016).
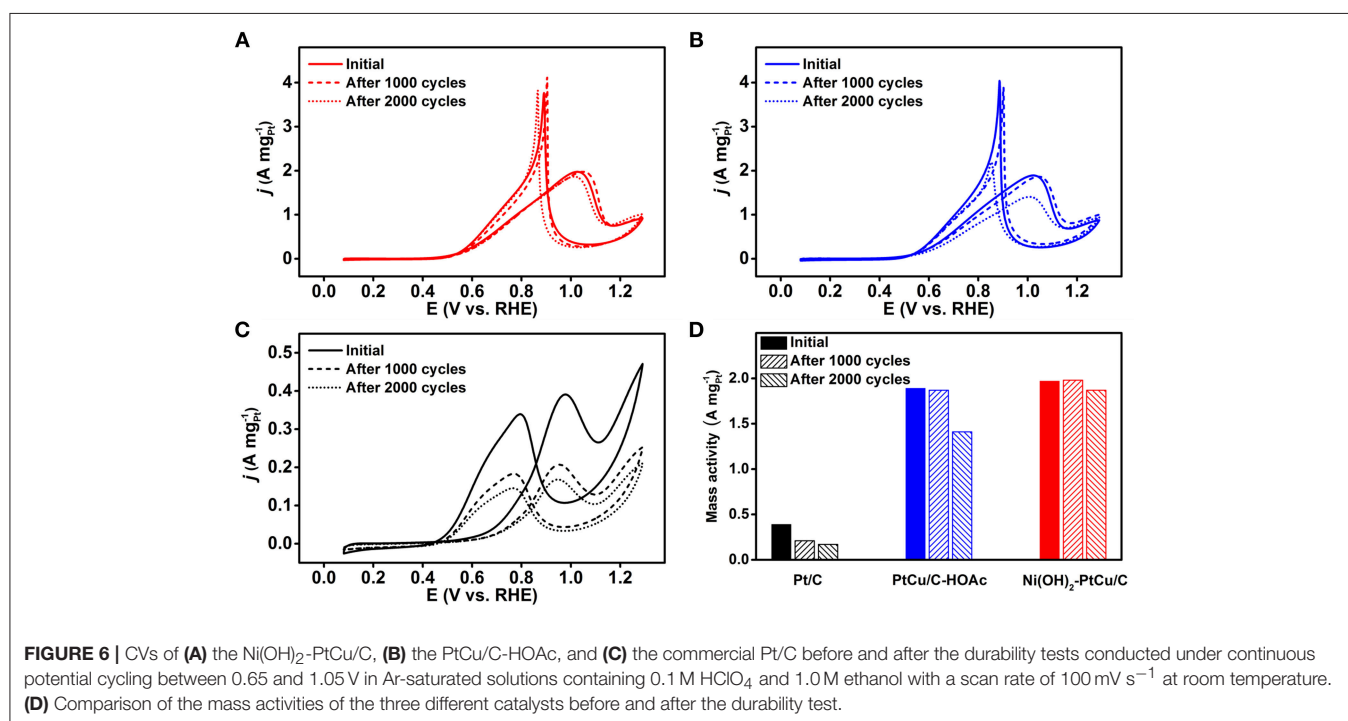
The resulting Ni(OH)$_2$-PtCu/C and PtCu/C-HOAc catalysts were evaluated as anodic oxidation electrocatalysts for EOR. For comparison, we benchmarked their electrochemical properties against the commercial Pt/C catalyst. Electrochemical measurements were conducted by using a potentiostats with three electrode system. The three different catalysts loaded working electrodes were pre-cleaned in Ar-saturated 0.1 M HClO$_4$ solutions between 0.08 and 1.20 V (vs. RHE) with a scan rate of 100 mV s^{-1} at room temperature. **Figure S2** presents TEM and EDS mapping images of Ni(OH)$_2$-PtCu/C after cleaning, showing similar morphology and composition to its status before cleaning. CVs were then recorded with the same potential range at a scan rate of 50 mV s^{-1} as shown in **Figure 4A**. The electrochemically active surface area (ECSA) of Pt was estimated by measuring the charge associated with hydrogen adsorption/desorption region in CVs and those are 27.27, 28.06, 60.29 m^2 g^{-1} for Ni(OH)$_2$-PtCu/C, PtCu/C-HOAc, and the commercial Pt/C, respectively (**Table 1**, Rudi et al., 2014; Kim et al., 2017). The lower ECSA of Ni(OH)$_2$-PtCu/C relative to that for the Pt/C is due to the bigger size and the presence of surface Ni(OH)$_2$ (Park et al., 2017). ECSA based on hydrogen adsorption/desorption region in CV is mainly responsible for Pt surface of catalysts. Therefore, the slight increase in ECSA with PtCu/C-HOAc in comparison to that of Ni(OH)$_2$-PtCu/C can be attributed to the removal of Ni(OH)$_2$ from the catalyst surface after HOAc treatment (Kavian et al., 2016). A key limiting factor for EOR catalysts is the intermediate species (i.e., CO) generated during the ethanol oxidation (Huang et al., 2015). Thus, electrochemical CO stripping measurement was conducted to examine the CO oxidation on the all presented catalysts. **Figure 4B** shows the CO stripping curves of Ni(OH)$_2$-PtCu/C, PtCu/C-HOAc, and the commercial Pt/C. The ECSAs were also calculated by CO stripping and those are 27.34, 30.85, 66.83 m^2 g^{-1} for Ni(OH)$_2$-PtCu/C, PtCu/C-HOAc, and the commercial Pt/C, respectively (Rudi et al., 2014; Kwon et al., 2018). The result is in accordance with the ECSA calculated by H adsorption/desorption. The onset potential for the CO stripping is usually used to prove the anti-CO poisoning property of the catalysts, in which lower potential values are related to higher CO tolerance (Zheng et al., 2015; Ahmad et al., 2019). The onset potential of the CO oxidation for Ni(OH)$_2$-PtCu/C catalyst appeared at 0.63 V, exhibiting more negative shift than that on the PtCu/C-HOAc (0.67 V) and Pt/C (0.80 V) catalysts. This result imply weaker CO adsorption strength on the Ni(OH)$_2$-PtCu/C and PtCu/C-HOAc catalysts than that on the Pt/C. (Xu et al., 2015; Sulaiman et al., 2017). As proposed by the *d*-band model, Pt alloying with Cu can induce lattice compression and thus down-shifting of the Pt *d*-band center, thereby weakening the CO adsorption energy (Yu et al., 2013; Hong et al., 2015; Zhang et al., 2015). In addition, since the CO stripping on Pt surface is sensitive to the surface arrangements, the octahedral shape of both the Ni(OH)$_2$-PtCu/C and PtCu/C-HOAc has a narrower distribution of CO binding strength, resulting in the
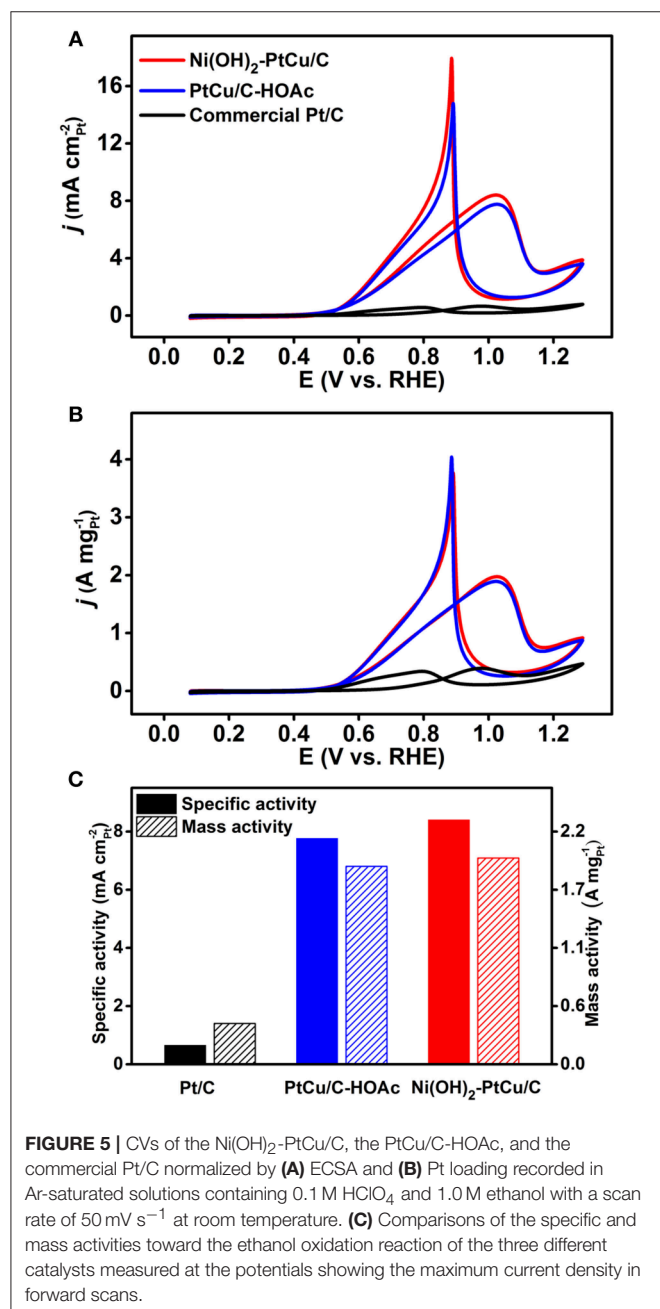
narrower CO oxidation peak as compared to spherical Pt/C enclosed by a mixed surface arrangement (Sulaiman et al., 2017). In the case of Ni(OH)$_2$-PtCu/C, existence of Ni(OH)$_2$ on Pt-Cu surfaces reduced the onset potential compared to the PtCu/C-HOAc owing to the presence of more OH adsorption sites to promote the CO oxidation, namely bifunctional effect (Erini et al., 2015; Xu et al., 2015). The CVs of the as-prepared catalysts for EOR were obtained in 0.1 M HClO$_4$ and 1.0 M ethanol solutions between 0.08 and 1.29 V with a scan rate of 50 mV s^{-1} at room temperature. In order to evaluate the EOR activity, the currents were normalized with ECSA and mass of Pt loading, indicating the specific and mass activities as shown in **Figures 5A,B**, respectively. The specific activity of the Ni(OH)$_2$-PtCu/C (8.40 mA cm^{-2}) at the potential showing highest current density in a forward scan exceeded those of the PtCu/C-HOAc (7.76 mA cm^{-2}) and the Pt/C (0.65 mA cm^{-2}), respectively. The EOR mass activity of Ni(OH)$_2$-PtCu/C is recorded the highest value of 1.97 A mg^{-1} compared to PtCu/C-HOAc (1.89 A mg^{-1}) and the Pt/C (0.39 A mg^{-1}) (**Figure 5C**). The enhanced EOR activity of the Ni(OH)$_2$-PtCu/C catalyst can be explained by the co-existence of surface Cu and Ni(OH)$_2$, which can sufficiently promote the water dissociation and thus formation of OH$_{ads}$ species to oxidize the toxic CO on the neighboring Pt surfaces (Erini et al., 2015; Zhang et al., 2015; Liu et al., 2017). Furthermore, the Ni(OH)$_2$-PtCu/C also exhibited a lower onset potential than that of the commercial Pt/C. The decrease in the onset potential probably indicates an enhancement in the kinetics of the EOR and may also hint toward an earlier C-C bond break (Erini et al., 2015). These results validate that the electrooxidation of ethanol on the Ni(OH)$_2$-PtCu/C is much easier. Although some of Ni(OH)$_2$ on the surface

was prone to dissolve in acidic media, the Ni(OH)$_2$-PtCu/C showed improved catalytic EOR performance and CO oxidation ability compared to the PtCu/C-HOAc, implying the influence of surface Ni(OH)$_2$. Consequently, the cooperation effect of Ni(OH)$_2$ and Cu leads to a significant increase in EOR activity and kinetic.

Chrono-amperometry (CA) curves of Ni(OH)$_2$-PtCu/C, PtCu/C-HOAc, and the commercial Pt/C were recorded at 0.67 V for 3,000 s to evaluate the CO tolerance on each catalyst (**Figure S3**) (Sulaiman et al., 2017). As the reaction proceeded for 3,000 s, the CA curves of Ni(OH)$_2$-PtCu/C showed relatively higher and more stable current densities compared to those of the PtCu/C-HOAc and the Pt/C. Because CO intermediate is stable under the continuous operation of EOR on Pt surfaces, this result indicates that the Ni(OH)$_2$-PtCu/C has a much higher CO tolerance than the PtCu/C-HOAc and the Pt/C. Long-term durability tests of Ni(OH)$_2$-PtCu/C, PtCu/C-HOAc, and the Pt/C for EOR were performed by applying cyclic potential sweeps between 0.65 and 1.05 V at 100 mV s^{-1} in an Ar-saturated solution containing 0.1 M HClO$_4$ and 1.0 M ethanol at room temperature. Then, CVs were recorded in a fresh Ar-saturated 0.1 M HClO$_4$ and 1.0 M ethanol solution between 0.08 and 1.29 V at 50 mV s^{-1} (**Figure 6**). After 1,000 cycles, the EOR mass activities of Ni(OH)$_2$-PtCu/C and PtCu/C-HOAc were similar to their initial values. In the case of Ni(OH)$_2$-PtCu/C, mass activity was slightly increased even after 1,000 cycles. Since the Ni(OH)$_2$ can be dissolved out from the Ni(OH)$_2$-PtCu/C during EOR cycles under acidic electrolyte, more exposed surface of Pt-Cu and optimized amount of Ni(OH)$_2$ can be assumed to show slightly enhanced EOR activity after 1,000 cycles (Cui et al., 2013b). After 2,000 cycles, EOR activities were degraded

FIGURE 6 | CVs of **(A)** the Ni(OH)$_2$-PtCu/C, **(B)** the PtCu/C-HOAc, and **(C)** the commercial Pt/C before and after the durability tests conducted under continuous potential cycling between 0.65 and 1.05 V in Ar-saturated solutions containing 0.1 M HClO$_4$ and 1.0 M ethanol with a scan rate of 100 mV s^{-1} at room temperature. **(D)** Comparison of the mass activities of the three different catalysts before and after the durability test.

for all catalysts. Mass activity of the commercial Pt/C catalyst was largely decreased about 57% compared to the initial value. However, both Ni(OH)$_2$-PtCu/C and PtCu/C-HOAc catalysts showed 5 and 25% degradation of mass activities to their initial values, respectively. All electrochemical results confirm that Ni(OH)$_2$-PtCu/C has improved catalytic activity and durability toward the ethanol electrooxidation.

CONCLUSION

We have successfully synthesized the Ni(OH)$_2$ decorated Pt-Cu octahedra in one-pot synthesis for EOR electrocatalysts in acidic electrolyte. CO gas was directly introduced in a reaction process as a capping agent on the PtCu(111) facet. Ni(OH)$_2$ was naturally deposited on the Pt-Cu alloy octahedra due to the difference of standard reduction potentials of Pt, Cu, and Ni. The presence of Ni(OH)$_2$ on the surface of catalysts and Pt-Cu alloy octahedra were confirmed by TEM, EDS, XPS, and XRD analyses. Electrochemical CO stripping experiment showed that enhanced CO tolerance of the Ni(OH)$_2$-PtCu/C compared to that of the PtCu/C-HOAc and the commercial Pt/C due to the existence of Ni(OH)$_2$ on the surface of Pt-Cu and incorporation of Pt with Cu. Pt-Cu alloy composition showed improved CO tolerance because of the down-shifted Pt d-band structure, thereby weakening the CO binding strength on the Pt. In this context, Ni(OH)$_2$-PtCu/C and PtCu/C-HOAc showed enhanced catalytic activity and durability toward ethanol electrooxidation in acidic electrolyte compared to the commercial Pt/C.

DATA AVAILABILITY

All datasets generated for this study are included in the manuscript/**Supplementary Files**.

AUTHOR CONTRIBUTIONS

YH, HK, and S-IC designed experiments, finished the synthesis and characterization analysis of materials, and carried out electrochemical experiment. HL and JK offered valuable suggestions to analysis of materials. YH, HK, and S-IC wrote the manuscript.

FUNDING

ACKNOWLEDGMENTS

SUPPLEMENTARY MATERIAL

The Supplementary Material for this article can be found online at: https://www.frontiersin.org/articles/10.3389/fchem.2019.00608/full#supplementary-material

REFERENCES

Ahmad, Y. H., Mohamed, A. T., Youssef, K. M., Kundu, S., Mkhoyan, K. A., and Al-Qaradawi, S. Y. (2019). Rational synthesis of ternary PtIrNi nanocrystals with enhanced poisoning tolerance for electrochemical ethanol oxidation. *Electrochem. Commun.* 101, 61–67. doi: 10.1016/j.elecom.2019.03.001

Ammam, M., and Easton, E. B. (2013). PtCu/C and Pt(Cu)/C catalysts: synthesis, characterization and catalytic activity towards ethanol electrooxidation. *J. Power Sources* 222, 79–87. doi: 10.1016/j.jpowsour.2012.07.143

Busó-Rogero, C., Herrero, E., and Feliu, J. M. (2014). Ethanol oxidation on Pt single-crystal electrodes: surface-structure effects in alkaline medium. *ChemPhysChem* 15, 2019–2028. doi: 10.1002/cphc.201402044

Chang, Q., Xu, Y., Duan, Z., Xiao, F., Fu, F., Hong, Y., et al. (2017). Structural evolution of sub-10 nm octahedral platinum-nickel bimetallic nanocrystals. *Nano Lett.* 17, 3926–3931. doi: 10.1021/acs.nanolett.7b01510

Choi, S.-I., Xie, S., Shao, M., Odell, J. H., Lu, N., Peng, H.-C., et al. (2013). Synthesis and characterization of 9 nm Pt-Ni octahedra with a record high activity of 3.3 A/mg$_{Pt}$ for the oxygen reduction reaction. *Nano Lett.* 13, 3420–3425. doi: 10.1021/nl401881z

Colmati, F., Tremiliosi-Filho, G., Gonzalez, E. R., Berná, A., Herrero, E., and Feliu, J. M. (2009). The role of the steps in the cleavage of the C–C bond during ethanol oxidation on platinum electrodes. *Phys. Chem. Chem. Phys.* 11, 9114–9123. doi: 10.1039/b907250k

Colmenares, L., Wang, H., Jusys, Z., Jiang, L., Yan, S., Sun, G. Q., et al. (2006). Ethanol oxidation on novel, carbon supported Pt alloy catalysts-model studies under defined diffusion conditions. *Electrochim. Acta* 52, 221–233. doi: 10.1016/j.electacta.2006.04.063

Cui, C., Ahmadi, M., Behafarid, F., Gan, L., Neumann, M., Heggen, M., et al. (2013a). Shape-selected bimetallic nanoparticle electrocatalysts: evolution of their atomic-scale structure, chemical composition, and electrochemical reactivity under various chemical environments. *Faraday Discuss.* 162, 91–112. doi: 10.1039/c3fd20159g

Cui, C., Gan, L., Heggen, M., Rudi, S., and Strasser, P. (2013b). Compositional segregation in shaped Pt alloy nanoparticles and their structural behaviour during electrocatalysis. *Nat. Mater.* 12, 765–771. doi: 10.1038/nmat3668

Dutta, A., and Ouyang, J. Y. (2015). Ternary NiAuPt nanoparticles on reduced graphene oxide as catalysts toward the electrochemical oxidation reaction of ethanol. *ACS Catal.* 5, 1371–1380. doi: 10.1021/cs501365y

Erini, N., Rudi, S., Beermann, V., Krause, P., Yang, R., Huang, Y., et al. (2015). Exceptional activity of a Pt-Rh-Ni ternary nanostructured catalyst for the electrochemical oxidation of ethanol. *ChemElectroChem* 2, 903–908. doi: 10.1002/celc.201402390

Ghavidel, M. R. Z., Videla, A. H. A. M., Specchia, S., and Easton, E. B. (2017). The relationship between the structure and ethanol oxidation activity of Pt-Cu/C alloy catalysts. *Electrochim. Acta* 230, 58–72. doi: 10.1016/j.electacta.2017.01.129

Hong, W., Wang, J., and Wang, E. (2015). Facile synthesis of PtCu nanowires with enhanced electrocatalytic activity. *Nano Res.* 7, 2308–2316. doi: 10.1007/s12274-015-0741-y

Hsieh, C.-T., and Lin, J.-Y. (2009). Fabrication of bimetallic Pt-M (M = Fe, Co, and Ni) nanoparticle/carbon nanotube electrocatalysts for direct methanol fuel cells. *J. Power Sources* 188, 347–352. doi: 10.1016/j.jpowsour.2008.12.031

Huang, M., Wu, W., Wu, C., and Guan, L. (2015). Pt$_2$SnCu nanoalloy with surface enrichment of Pt defects and SnO2 for highly efficient electrooxidation of ethanol. *J. Mater. Chem. A* 3, 4777–4781. doi: 10.1039/C4TA06695B

Kang, Y., Pyo, J. B., Ye, X., Diaz, R. E., Gordon, T. R., Stach, E. A., et al. (2013). Shape-controlled synthesis of Pt nanocrystals: the role of metal carbonyls. *ACS Nano* 7, 645–653. doi: 10.1021/nn3048439

Kang, Y., Ye, X., and Murray, C. B. (2010). Size- and shape-selective synthesis of metal nanocrystals and nanowires using CO as a reducing agent. *Angew. Chem. Int. Ed.* 49, 6156–6159. doi: 10.1002/anie.201003383

Kavian, R., Choi, S.-I., Park, J., Liu, T., Peng, H.-C., Lu, N., et al. (2016). Pt-Ni octahedral nanocrystals as a class of highly active electrocatalysts toward the hydrogen evolution reaction in an alkaline electrolyte. *J. Mater. Chem. A* 4, 12392–12397. doi: 10.1039/C6TA05411K

Kim, H. J., Ahn, Y.-D., Kim, J., Kim, K.-S., Jeong, Y. U., Hong, J. W., et al. (2019). Surface elemental distribution effect of Pt-Pb hexagonal nanoplates for electrocatalytic methanol oxidation reaction. *Chin. J. Catal.* 40. Available online at: http://www.cjcatal.org/EN/article/searchArticle.do

Kim, H. J., Ruqia, B., Kang, M. S., Lim, S. B., Choi, R., Nam, K., et al. (2017). Shape-controlled Pt nanocubes directly grown on carbon supports and their electrocatalytic activity toward methanol oxidation. *Sci. Bull.* 62, 943–949. doi: 10.1016/j.scib.2017.05.029

Koper, M. T. (2011). Structure sensitivity and nanoscale effects in electrocatalysis. *Nanoscale* 3, 2054–2073. doi: 10.1039/c0nr00857e

Kowal, A., Li, M., Shao, K., Sasaki, K., Vukmirovic, M. B., and Zhang, J. (2009). Ternary Pt/Rh/SnO$_2$ electrocatalysts for oxidizing ethanol to CO$_2$. *Nat. Mater.* 8, 325–330. doi: 10.1038/nmat2359

Kwon, H., Kabiraz, M. K., Park, J., Oh, A., Baik, H., Choi, S.-I., et al. (2018). Dendrite-embedded platinum-nickel multiframes as highly active and durable electrocatalyst toward the oxygen reduction reaction. *Nano Lett.* 18, 2930–2936. doi: 10.1021/acs.nanolett.8b00270

Lai, S. C., and Koper, M. T. (2008). Electro-oxidation of ethanol and acetaldehyde on platinum single-crystal electrodes. *Faraday Discuss.* 140, 399–416. doi: 10.1039/B803711F

Li, G., and Pickup, P. G. (2006). Analysis of performance losses of direct ethanol fuel cells with the aid of a reference electrode. *J. Power Sources* 161, 256–263. doi: 10.1016/j.jpowsour.2006.03.071

Liu, T., Li, C., and Yuan, Q. (2018). Facile synthesis of PtCu alloy/graphene oxide hybrids as improved electrocatalysts for alkaline fuel cells. *ACS Omega* 3, 8724–8732. doi: 10.1021/acsomega.8b01347

Liu, T., Wang, K., Yuan, Q., Chen, Z., Wang, Y., Zhang, Q., et al. (2017). Monodispersed sub-5.0 nm PtCu nanoalloys as enhanced bifunctional electrocatalysts for oxygen reduction reaction and ethanol oxidation reaction. *Nanoscale* 9, 2963–2968. doi: 10.1039/C7NR00193B

Moulder, J. F. (1992). *Handbook of X-Ray Photoelectron Spectroscopy: A Reference Book of Standard Spectra for Identification and Interpretation of XPS Data.* Waltham: Perkin-Elmer Corporation.

Neto, A. O., Dias, R. R., Tusi, M. M., Linardi, M., and Spinace, E. V. (2007). Electro-oxidation of methanol and ethanol using PtRu/C, PtSn/C and PtSnRu/C electrocatalysts prepared by an alcohol-reduction process. *J. Power Sources* 166, 87–91. doi: 10.1016/j.jpowsour.2006.12.088

Nosheen, F., Zhang, Z.-C., Zhuang, J., and Wang, X. (2013). One-pot fabrication of single-crystalline octahedral Pt-Cu nanoframes and their enhanced electrocatalytic activity. *Nanoscale* 5, 3660–3663. doi: 10.1039/c3nr00833a

Ozoemena, K. I. (2016). Nanostructured platinum-free electrocatalysts in alkaline direct alcohol fuel cells: catalyst design, principles and applications. *RSC Adv.* 6, 89523–89550. doi: 10.1039/C6RA15057H

Park, J., Kabiraz, M. K., Kwon, H., Park, S., Baik, H., Choi, S.-I., et al. (2017). Radially phase segregated PtCu@PtCuNi dendrite@frame nanocatalyst for the oxygen reduction reaction. *ACS Nano* 11, 10844–10851. doi: 10.1021/acsnano.7b04097

Rudi, S., Cui, C., Gan, L., and Strasser, P. (2014). Comparative study of the Electrocatalytically Active Surface Areas (ECSAs) of Pt alloy nanoparticles evaluated by Hupd and CO-stripping voltammetry. *Electrocatalysis* 5, 408–418. doi: 10.1007/s12678-014-0205-2

Solla-Gullon, J., Vidal-Iglesias, F. J., and Feliu, J. M. (2011). Shape dependent electrocatalysis. *Annu. Rep. Prog. Chem. Sect. C* 107, 263–297. doi: 10.1039/c1pc90010b

Sulaiman, J. E., Zhu, S., Xing, Z., Chang, Q., and Shao, M. (2017). Pt-Ni octahedra as electrocatalysts for the ethanol electrooxidation reaction. *ACS Catal.* 7, 5134–5141. doi: 10.1021/acscatal.7b01435

Vigier, F., Coutanceau, C., Hahn, F., Belgsir, E. M., and Lamy, C. (2004). On the mechanism of ethanol electro-oxidation on Pt and PtSn catalysts: electrochemical and *in situ* IR reflectance spectroscopy studies. *J. Electroanal. Chem.* 563, 81–89. doi: 10.1016/j.jelechem.2003.08.019

Wang, H., Jusys, Z., and Behm, R. J. (2006). Ethanol electro-oxidation on carbon-supported Pt, PtRu and Pt3Sn catalysts: A quantitative DEMS study. *J. Power Sources* 154, 351–359. doi: 10.1016/j.jpowsour.2005.10.034

Wang, Y., Zou, S., and Cai, W.-B. (2015). Recent advances on electro-oxidation of ethanol on Pt- and Pd-based catalysts: from reaction mechanisms to catalytic materials. *Catalysts* 5, 1507–1534. doi: 10.3390/catal5031507

Xia, B. Y., Wang, B., Wu, H. B., Liu, Z., Wang, X., and Lou, X. W. D. (2012). Sandwich-structured TiO$_2$-Pt-graphene ternary hybrid electrocatalysts with high efficiency and stability. *J. Mater. Chem.* 22, 16499–16505. doi: 10.1039/c2jm32816j

Xu, H., Ding, L.-X., Feng, J.-X., and Li, G.-R. (2015). Pt/Ni(OH)$_2$-NiOOH/Pd multi-walled hollow nanorod arrays as superior electrocatalysts for formic acid electrooxidation. *Chem. Sci.* 6, 6991–6998. doi: 10.1039/C5SC02544C

Xu, Y., and Zhang, B. (2014). Recent advances in porous Pt-based nanostructures: synthesis and electrochemical applications. *Chem. Soc. Rev.* 43, 2439–2450. doi: 10.1039/c3cs60351b

Yu, X., Wang, D., Peng, Q., and Li, Y. (2013). PtM (M=Cu, Co, Ni, Fe) nanocrystals: from small nanoparticles to wormlike nanowires by oriented attachment. *Chem. Eur. J.* 19, 233–239. doi: 10.1002/chem.201203332

Zhang, P., Dai, X., Zhang, X., Chen, Z., Yang, Y., Sun, H., et al. (2015). One-pot synthesis of ternary Pt-Ni-Cu nanocrystals with high catalytic performance. *Chem. Mater.* 27, 6402–6410. doi: 10.1021/acs.chemmater.5b02575

Zhang, Z., Luo, Z., Chen, B., Wei, C., Zhao, J., Chen, J., et al. (2016). Ont-pot synthesis of highly anisotropic five-fold-twinned PtCu nanoframes used as a bifunctional electrocatalyst for oxygen reduction and methanol oxidation. *Adv. Mater.* 28, 8712–8717. doi: 10.1002/adma.201603075

Zhao, T.-T., Wang, H., Han, X., Jiang, K., Lin, H., Xie, Z., et al. (2016). A comparative investigation of electrocatalysis at Pt monolayers on shape-controlled Au nanocrystals: facet effect *versus* strain effect. *J. Mater. Chem. A* 4, 15845–15850. doi: 10.1039/C6TA06794H

Zheng, J., Cullen, D. A., Forest, R. V., Wittkopf, J., Zhuang, Z., Sheng, W., et al. (2015). Platinum–ruthenium nanotubes and platinum–ruthenium coated copper nanowires as efficient catalysts for electro-oxidation of methanol. *ACS Catal.* 5, 1468–1474. doi: 10.1021/cs501449y

Zhou, W., Zhou, Z., Song, S., Li, W., Sun, G., Tsiakaras, P., et al. (2003). Pt based anode catalysts for direct ethanol fuel cells. *Appl. Catal. B Environ.* 46, 273–285. doi: 10.1016/S0926-3373(03)00218-2

Zhu, W., Ke, J., Wang, S.-B., Ren, J., Wang, H.-H., Zhou, Z.-Y., et al. (2015). Shaping single-crystalline trimetallic Pt–Pd–Rh nanocrystals toward high-efficiency C–C splitting of ethanol in conversion to CO2. *ACS Catal.* 5, 1995–2008. doi: 10.1021/cs5018419